Biogeosciences Discuss., 8, 4985–5017, 2011
www.biogeosciences-discuss.net/8/4985/2011/
doi:10.5194/bgd-8-4985-2011


Biogeosciences Discussions



# Remote sensing of size structure of phytoplankton communities using optical properties of the Chukchi and Bering Sea shelf region

**A. Fujiwara**[1], **T. Hirawake**[1,2], **K. Suzuki**[3,4], **and S.-I. Saitoh**[1,2]

[1]Graduate Scholl of Fisheries Sciences, Hokkaido University, 3-1-1 Minato-cho, Hakodate, Hokkaido 041-8611, Japan
[2]Faculty of Fisheries Sciences, Hokkaido University, 3-1-1 Minato-cho, Hakodate, Hokkaido 041-8611, Japan
[3]Graduate School of Environmental Science, Hokkaido University, North 10 West 5, Kita-ku, Sapporo, Hokkaido 060-0810, Japan
[4]Faculty of Environmental Earth Science, Hokkaido University, North 10 West 5, Kita-ku, Sapporo, Hokkaido 060-0810, Japan

Received: 22 April 2011 – Accepted: 3 May 2011 – Published: 23 May 2011

Correspondence to: A. Fujiwara (amane@salmon.fish.hokudai.ac)

Published by Copernicus Publications on behalf of the European Geosciences Union.







## Abstract

Recent ocean warming and subsequent sea ice decline resulting from climate change could affect the northward shift of the ecosystem structure in the Chukchi Sea and Bering Sea shelf region. The size structure of phytoplankton communities provides an index of trophic levels that is crucial to understanding the mechanisms underlying such ecosystem changes and their implications for the future. This study proposes a new ocean color algorithm for deriving this characteristic by using the region's optical properties. The size derivation model (SDM) estimates the phytoplankton size index $F_L$ on the basis of size-fractionated chlorophyll-*a* (chl-*a*) using the light absorption coefficient of phytoplankton, $a_{ph}(\lambda)$, and the backscattering coefficient of suspended particles including algae, $b_{bp}(\lambda)$. $F_L$ was defined as the ratio of algal biomass attributed to cells larger than 5 µm to the total. It was expressed by a multiple regression model using the $a_{ph}(\lambda)$ ratio, $a_{ph}(488)/a_{ph}(555)$, which varies with phytoplankton pigment composition, and the spectral slope of $b_{bp}(\lambda)$, $\gamma$, which is an index of the mean suspended particle size. A validation study demonstrated that the SDM successfully derived an $F_L$ value of 69 % within an error range of ±20 % for unknown data. The spatial distributions of $F_L$ for the cold August of 2006 and the warm August of 2007 were compared to examine application of the SDM to satellite remote sensing. The results suggested that phytoplankton size was responsive to changes in sea surface temperature. Further analysis of satellite-derived $F_L$ values and other environmental factors can advance our understanding of ecosystem structure changes in the shelf region of the Chukchi and Bering Seas.

## 1 Introduction

The Chukchi Sea, located at the western edge of the Arctic Ocean, and the Bering Sea, located at the northern edge of the Pacific Ocean, are connected by the Bering Strait. The continental shelf spreads north and south of the Bering Strait for 2000 km,





BGD
8, 4985–5017, 2011



and the water depths are shallower than 50 m in most of the region. Three types of water masses flow through the region: Alaskan Coastal Water (ACW), Anadyr Water (AW), and Bering Shelf Water (BSW). ACW has a high temperature and low salinity due to fresh water input; it passes along the western coast of Alaska and flows out to the Beaufort Sea (Coachman et al., 1975). AW, which flows along the eastern coast of Siberia, has a low temperature and high salinity, and supplies large amounts of nutrients to the Bering Sea and Bering Strait (Coachman et al., 1975). BSW flows between AW and ACW. Its water density is very similar to that of AW, so they become well mixed when they pass through the Bering Strait (Grebmeier et al., 1988). This mixed water, called Bering Shelf–Anadyr Water (BSAW) (Grebmeier et al., 1988) supplies nutrient-rich water to the Southern Chukchi Sea.

The shelf region influenced by BSAW is known as one of the most highly productive regions in the world's oceans. The maximum primary production reaches 840 g C $m^{-2}$ $y^{-1}$ (Springer and McRoy, 1993). Organic carbon produced at the surface and subsurface layers by phytoplankton is exported efficiently to the bottom because of the shallow depth and the low grazing impact of zooplankton (Grebmeier et al., 1988; Feder et al., 2005), and supports a high benthic biomass in the region. Consequently, large benthic feeders at high trophic levels such as gray whales (*Eschrichtius robustus*) and walrus (*Odobenus rosmarus divergens*) also congregate here (Feder et al., 2005). This unique ecosystem structure with a significantly short food chain forms because of the tightly linked energy transport between phytoplankton and benthos (Grebmeier et al., 2006b).

Recently, remotely sensed microwave observations by satellite have indicated that the sea-ice area in the Arctic Ocean is declining annually (e.g., Comiso et al., 2008; Parkinson and Cavalieri, 2008). This is especially significant in September when the largest open water area occurs (e.g., Comiso, 2002; Shimada et al., 2006). Shimada et al. (2006) noted that a recent reduction in sea-ice cover is due to increasing heat flux from Pacific summer water. Woodgate et al. (2006) also showed that the increase in heat flux in 2001–2004 is attributable to a volume flux increase of Pacific water,





BGD
8, 4985–5017, 2011



corresponding to ~640 000 km$^2$ of 1-m-thick ice melting in these four years. Shimada et al. (2006) suggested that the reduction in sea ice causes less ice-productive conditions in the Western Arctic and forms a positive feedback mechanism toward further sea-ice reduction.

Various effects of reduced sea ice and increased temperature on the marine ecosystem have been reported. Arrigo et al. (2008) and Pabi et al. (2008), for example, suggested that annual primary production in the Arctic Ocean has been increasing owing to increases in the algal growth season and habitat area resulting from diminishing sea-ice area. Grebmeier et al. (2006a) note that the tightly linked phytoplankton–benthos ecosystem structure (pelagic–benthic type) is forced to shift northward because of ocean warming. Consequently, the ecosystem structure switches from short-chained pelagic–benthic type to a pelagic–pelagic (algae–zooplankton) type having more trophic levels. Although the ecosystem structure in the study region is likely to be in a dramatic transitional phase right now, it is still unknown how the distribution of phytoplankton community structure varies owing to environmental change. Because phytoplankton is the basis of the ecosystem, its community structure (size or taxonomic composition) can be an important factor for assessing the response of the ecosystem to environmental change. Thus, it is necessary to clarify the spatial and temporal variability of the phytoplankton distribution in the shelf region.

The first satellite ocean color sensor, the Coastal Zone Color Scanner (CZCS), was launched in 1978 and provided high spatiotemporal data until 1986. Sensors such as the Sea-viewing Wide Field-of-view Sensor (SeaWiFS) and Moderate Resolution Spectroradiometer (MODIS) have also provided higher-quality ocean color data. The most successful result of satellite observations has been the provision estimates of chlorophyll-*a* (chl-*a*) concentration, which is an index of phytoplankton biomass, over wide spatial and temporal scales. Seasonal phytoplankton cycles have been clarified at not only regional but also global scales (Yoder and Kennelly, 2006). Chl-*a* is still the main index provided by ocean color satellites for improving oceanographic knowledge. Recently, several attempts have also been made to develop methods that use





BGD
8, 4985–5017, 2011



ocean color data to estimate the dominant distribution of Phytoplankton functional types (PFTs), including phytoplankton size classes at large spatial scales (e.g., Sathyendranath et al., 2004; Alvain et al., 2005; Uitz et al., 2006; Ciotti and Bricaud, 2006; Mouw and Yoder, 2010; Brewin et al., 2010). It has recently been established that different phytoplankton groups make different contributions to large-scale-biogeochemical cycles in the ocean; these groups are called PFTs. For example, there are nitrogen fixing groups (Zehr and Carpenter, 2000) and groups that produce dimethylsulfide (DMS) (a precursor of cloud condensation nuclei) (Turner et al., 1988); even the carbon-fixating efficiency varies among groups (Lochte et al., 1993). Since it is an important factor in determining the number of trophic levels of a regional ecosystem (Lalli and Parsons, 1995), dominant cell size of phytoplankton is also described as a PFT.

The use of the inherent optical properties (IOPs) (absorption and backscattering) of seawater is the principle method of estimating PFT composition optically because these properties vary with the PFT composition of the water. The IOPs influenced by PFT composition affect the property of water-leaving radiance $L_w$ (see Table 1 for symbols), which can be observed directly by satellite sensors. Several studies have suggested that quantifying the relationship between PFT composition and IOPs allows us to estimate their distribution, especially in Case 1 waters (Morel and Prieur, 1977). Fishwick et al. (2006), for instance, showed a significant difference in the spectral ratio of the absorption coefficient $a_{ph}(\lambda)$, i.e., the ratio of $a_{ph}(676)$ to $a_{ph}(440)$ ($a_{ph}[676]/a_{ph}[440]$), among dominant phytoplankton groups, which coincides with the ratio of the accessory pigments to chl-*a* or maximum photosynthetic quantum efficiency. They suggested that the ratio of $a_{ph}(\lambda)$ at red light to that at blue light should be an indicator for determining the dominance of PFTs, at least for the Benguela ecosystem. On the other hand, the spectral shape of the particle backscattering coefficient $b_{bp}(\lambda)$ is known to vary with the mean size of suspended particles in the water (e.g., Bricaud and Morel, 1986; Stramski et al., 2001; Vaillancourt et al., 2004). Then, Montes-Hugo et al. (2008) assessed the relationship between the spectral slope of $b_{bp}(\lambda)$, $\gamma$, and phytoplankton cell size for the Western Antarctic Peninsula region. They





BGD
8, 4985–5017, 2011



showed that $\gamma$ could act as an optical index of the dominance of microphytoplankton (> 20 µm in size) bloom.

On the other hand, direct satellite measurement of the IOPs is impossible; therefore, they must be estimated using $L_w$. To apply an IOP-based PFT estimation model to satellite remote sensing data, other optical models for estimating IOPs are required. Several IOP models have been reported (e.g., Carder et al., 1999; Sathyendranath et al., 2001; Lee et al., 2002; Smyth et al., 2006). Note that IOPs are specific to regional water and vary with the water components, such as phytoplankton taxa, suspended particles, or dissolved organic materials. Therefore, IOP models should be fully validated in the area where they are applied (Wang et al., 2005). Sathyendranath et al. (2004) reported, for example, that the algorithm developed for the North West Atlantic Zone to identify diatom blooms, should be tuned when it is applied to other regions because of variations in the optical properties of diatoms. Wang and Cota (2003) also suggested that proposed IOP models should be empirically tuned for the study regions before their use. Little is known about the quantitative relationship between PFTs and IOPs in the Chukchi and Bering Sea shelf region. Thus, it is necessary to quantify the optical properties of phytoplankton assemblages and other components of the water in order to use satellite observation to monitor the spatial distribution of PFTs in the area.

To elucidate the mechanism of ecosystem changes due to recent environmental changes in the Chukchi and Bering Sea shelf, we emphasize the importance of monitoring the temporal and spatial distribution of phytoplankton-size-specific biomass, which is a major factor in determining the number of trophic levels. However, it is not clear how variations in phytoplankton size structure affect the optical properties of seawater in the region. Moreover, an optical model for estimating phytoplankton size structure suitable for the area has not yet been developed. We therefore developed a size derivation model (SDM) for estimating the phytoplankton size structure index ($F_L$) (defined as the fraction of larger-celled phytoplankton (> 5 µm) in the total assemblage) by assessing the relationship between $F_L$ and the optical properties (absorption and backscattering). In this paper, we propose an SDM that adopts multiple regression





BGD
8, 4985–5017, 2011



models using two different optical variables and show the accuracy of phytoplankton size estimates. Finally, we evaluated whether the model can be used to discuss and improve biogeochemical knowledge.

## 2 Materials and methods

### 2.1 Study sites

Data for the present study were sampled in the continental shelf region of the Chukchi and Bering Seas (Fig. 1). In situ data for developing the SDM were sampled during a cruise of the T/S *Oshoro-maru* (Hokkaido University) in summer 2007 (OS180 cruise). There were 22 sampling stations, 10 in the Bering Sea and 12 in the Chukchi Sea (Fig. 1). In addition, samples used to validate the SDM accuracy were collected during the cruises of the T/S *Oshoro-maru* in the early summer 2008 (OS190 cruise), the R/V *Mirai* (Japan Agency for Marine–Earth Science and Technology, JAMSTEC) in the late summer 2009 (MR09-03 cruise) and 2010 (MR10-05 cruise), and R/V *Hakuho-maru* (JAMSTEC) in summer 2009 (KH09-4 cruise). There were 2, 14, 31, and 8 sampling stations in the study region, respectively, for each cruise (Fig. 1).

### 2.2 Size fractionated phytoplankton pigments analysis

The biomass of phytoplankton assemblages was defined in terms of chl-*a* level. The concentrations of size-fractionated chl-*a* and other phytoplankton pigments for SDM development were determined by high-performance liquid chromatography (HPLC). Water samples for HPLC were collected from six fixed depths, 0, 10, 20, 30, 50, and 75 m or six light depths (100 %, 50 %, 25 %, 10 %, 5 %, and 1 % penetration of surface photosynthetically available radiation) determined by a scalar light sensor (LI-193SA, LI-COR) with CTD/rosette samplers. The samples were passed through 20- and 5-µm nylon mesh filters and Whatman GF/F filters (47 mm in diameter) under gentle vacuum (< 0.013 MPa). Filters were stored in liquid nitrogen until analysis





BGD
8, 4985–5017, 2011



in the laboratory. Filter samples were broken into pieces and soaked in 5 ml $N'N$-dimethylformamide (DMF) containing canthaxanthin as an internal standard. The extraction and detection of phytoplankton pigments are described in detail in Suzuki et al. (2005). We selected seven major pigments on the basis of comparable studies that referred to the relationship between cell size and pigment composition (Vidussi et al., 2001): fucoxanthin (Fuco), peridinin (Peri), 19′-hexanoyloxyfucoxanthin (19′-HF), 19′-butanoyloxyfucoxanthin (19′-BF), alloxanthin (Allo), zeaxanthin (Zea), total chlorophyll-*b* (chl-*b*), and also chl-*a*. The pigments are typical of phytoplankton groups and are often used as biomarkers (e.g., Jeffrey and Vesk, 1997, Table 2). Following the method of Aiken et al. (2007) as described in Table 2, we simply estimated the fraction of four major phytoplankton assemblages (diatoms, dinoflagellates, nano-flagellates and prokaryotes) in the total algal biomass using HPLC pigment composition. For SDM validation, size-fractionated chl-*a* concentrations at the surface sampled during the OS190, MR09-03, KH09-4, and MR10-05 cruises were determined by a fluorometric method with a Turner Designs model 10-AU fluorometer (Welschmeyer et al., 1994). The sample water was passed through 20- and 5-µm nylon mesh filters and GF/F filters (47 mm in diameter) on the OS190, 10- and 2-µm pore-size Whatman Nuclepore and GF/F filters on the KH09-4, and 10-, 5-, 2-µm Nuclepore and GF/F filters on the MR09-03 and the MR10-05.

We define the phytoplankton size index $F_L$ as

$$F_L = \frac{\text{chl-}a_{>5\,\mu\text{m}}}{\text{chl-}a_{\text{total}}} \times 100\,[\%], \quad (1)$$

where chl-$a_{>5\,\mu\text{m}}$ and chl-$a_{\text{total}}$ indicate chl-*a* larger than 5 µm and the sum of chl-*a* of all sizes, respectively. Chl-*a* was not measured using a mesh with 5-µm pore size on KH09-4; therefore chl-*a* larger than 10 µm (chl-$a_{>10\,\mu\text{m}}$) was converted to chl-$a_{>5\,\mu\text{m}}$ by an empirical equation using surface-size-fractionated chl-*a* data obtained on MR09-03 and MR10-05,

$$\text{chl-}a_{>5\,\mu\text{m}} = a + b\,\text{chl-}a_{>10\,\mu\text{m}} + c\,\text{chl-}a^2_{>10\,\mu\text{m}} + d\,\text{chl-}a^3_{>10\,\mu\text{m}}, \quad (2)$$





BGD
8, 4985–5017, 2011



where $a = 0.003$, $b = 1.504$, $c = -1.080$, and $d = 0.605$. These two chl-*a* values were tightly co-varied ($r^2 = 0.97$).

### 2.3 Bio-optical observations

Absorption coefficients and backscattering coefficients were obtained as IOPs in this study. Samples used for determining the spectral absorption coefficients of suspended particles $a_p(\lambda)$ and of colored dissolved organic matter (CDOM) $a_{CDOM}(\lambda)$ were taken from the same water as the HPLC samples. The samples for measuring $a_p(\lambda)$ (200–4000 ml) and $a_{CDOM}$ (250 ml) were both gently filtered (< 0.013 MPa): through a Whatman GF/F filter (25 mm in diameter) for $a_p(\lambda)$ and through a Whatman Nuclepore filter with 0.2-μm pore size (47 mm in diameter) for $a_{CDOM}(\lambda)$. The optical density (OD, dimensionless) of the collected particles was measured immediately using an MPS2450 spectrophotometer (Shimadzu) between 350 and 750 nm in 1 nm increments. A GF/F-filtered sample was rinsed and soaked in methanol to extract pigments (Kishino et al., 1985), and the OD of non-algal particles (NAPs) was re-measured. Then the absorption coefficients of total suspended particles, $a_p(\lambda)$ and $a_{NAP}(\lambda)$, were calculated, using the correction of the path length amplification due to multiple scattering inside the filter given in Cleveland and Weidemann (1993). The absorption of phytoplankton cells, $a_{ph}(\lambda)$, was obtained by subtracting $a_{NAP}(\lambda)$ from $a_p(\lambda)$. The OD of filtered samples used to determine $a_{CDOM}(\lambda)$ was measured immediately with the MPS2450 instrument and was calculated as $a_{CDOM}(\lambda)$ by a the method described in a SeaWiFS technical report (Pegau et al., 2003).

The vertical distribution (0–80 m) of the volume scattering functions $\beta(\theta)$ for three angles ($\theta = 100$, 125, and 150°) at three wavelengths (440, 531, and 660 nm) was also measured using an in-water VSF meter (Eco-VSF3P, WET Labs). This measurement was done immediately after water sampling. The particle backscattering coefficient $b_{bp}(\lambda)$ was estimated from $\beta(100)$ using a $\chi$ value that is a factor proportionally





BGD
8, 4985–5017, 2011



between $b_{bp}(\lambda)$ and $\beta(\theta)$, as proposed by Maffione and Dana (1997),

$$b_{bp}(\lambda) = 2\pi\chi\beta(100^\circ, \lambda), \tag{3}$$

where $\chi = 0.86$ according to the value obtained empirically in Sullivan and Twardowski (2009). The general spectral shape of $b_{bp}(\lambda)$ can be approximated functionally (e.g., Smith and Baker, 1981; Sathyendranath et al., 2001):

$$b_{bp}(\lambda) = b_{bp}(\lambda_0)\left(\frac{\lambda_0}{\lambda}\right)^{\gamma} \tag{4}$$

where $\lambda_0$ is a reference wavelength, which is set to 555 nm in this study, and $\gamma$ is the spectral slope. We determined the values of $\gamma$ for the water at each sampled depth by a least squares method fitted to $b_{bp}(\lambda)$ at three wavelengths.

Vertical profiles of downwelling irradiance $E_d(\lambda)$ and upwelling radiance $L_u(\lambda)$ were measured. These data were collected using two optical instruments, a HyperPro free-fall profiler (Satlantic, Inc.) during the OS180 and OS190 cruises, and a PRR800/810 free-fall profiler (Biospherical Instruments Inc.) during the MR09-03, KH09-4, and MR10-05 cruises. The spectral remote sensing reflectance $R_{rs}(\lambda)$ was calculated as the ratio of the water-leaving radiance $L_w(\lambda)$ to $E_d(\lambda)$ just above the water (Darecki and Stramski, 2004),

$$R_{rs}(\lambda) = \frac{L_w(\lambda, 0^+)}{E_d(\lambda, 0^+)} = 0.544\frac{L_u(\lambda, 0^-)}{E_d(\lambda, 0^+)}, \tag{5}$$

where 0.544 is a water–air interface propagation factor.

### 2.4 Quantification of phytoplankton size and community structure using IOPs

We investigated the quantitative relationships between phytoplankton size structure index $F_L$ and the IOPs. First, we assessed the relationship between $F_L$ and the absorption properties. Several studies have already established that the ratio of $a_{ph}(\lambda)$ at





BGD
8, 4985–5017, 2011



different wavelengths, such as blue and red light, can be used as an indicator to assess the abundance of accessory pigments relative to total chl-*a*. Accessory pigment composition varies with the phytoplankton taxa and is related to nutrient conditions (e.g., Ciotti et al., 2002; Fishwick et al., 2006); large-celled diatoms tend to be dominant in eutrophic regimes, and small prokaryotes are important in oligotrophic regimes (Chisholm, 1992).

On the other hand, we also evaluated the relationship between $F_L$ and $\gamma$ in accordance with the method and theories proposed by Montes-Hugo et al. (2008). According to the Mie theory, $\gamma$ increases as the mean particle size decreases. To investigate the variation in particle backscattering with algal cell size composition, $b_{bp}(\lambda)$ data from turbid water were omitted. Turbid water was defined as that in which the contribution of $a_{NAP}(443)$ to the total absorption coefficient $a_t(443)$ was greater than that of $a_{ph}(443)$. Then, we attempted to quantify $F_L$ empirically using these IOPs.

### 2.5 SDM validations and application

To apply the SDM to satellite remote sensing estimation of the IOPs, $a_{ph}(\lambda)$ and $\gamma$ are needed as model inputs. The $a_{ph}(\lambda)$ value at the sea surface was derived from $R_{rs}(\lambda)$ using the quasi-analytical algorithm (QAA) proposed by Lee et al. (2002). The QAA uses several calculation processes and yields $a_{ph}(\lambda)$ as the final product. We used the latest version of the QAA (version 5, QAA-v5) (Lee et al., 2009), in which the empirical calculation steps, Tables 2 and 3 in Lee et al. (2002), have been updated. For the calculation step 8 of the QAA, the spectral slope $S$ of $a_{dg}(\lambda)$ (the sum of the $a_{CDOM}[\lambda]$ and $a_{NAP}[\lambda]$ values) was tuned for the study region empirically using data obtained on OS180. On the other hand, $\gamma$ was derived from $R_{rs}(488)/R_{rs}(555)$, which was used to derive $\gamma$ in Lyon and Hoge (2006):

$$\gamma = 2.092 + 9.577R + 17.67R^2 + 11.10R^3, \quad (6)$$

where $R = \ln(R_{rs}(488)/R_{rs}(555))$. The coefficients in Eq. (6) were empirically determined using in situ $\gamma$ and $R_{rs}(\lambda)$ values measured with the VSF3P and Hyper-OCR





BGD
8, 4985–5017, 2011



instruments. The estimation performance of the SDM was also examined using $R_{rs}(\lambda)$ data obtained during the OS190, MR09-03, KH09-4, and MR10-05 cruises.

We applied the SDM to satellite data. The MODIS/Aqua Level 3 binned remote sensing reflectance $R_{rs}(\lambda)$ and sea surface temperature (SST) data were downloaded from the Distributed Active Archive Center (DAAC) of Goddard Space Flight Center (GSFC), NASA. Monthly averaged data for August 2006 and August 2007 were obtained. The input parameters for the SDM were derived from the $R_{rs}(\lambda)$ data at wavelengths of 412, 443, 488, 555, and 667 nm using QAA-v5 and Eq. (6). Then, $F_L$ was derived for each frame of the remotely sensed satellite images. The satellite chl-*a* was also calculated from $R_{rs}(\lambda)$ using the Arctic OC4L algorithm (Eq. 7) (Cota et al., 2004) which is optimized for highly packaged data resulting from large, shade-acclimated phytoplankton at the latitudes (Cota et al., 2003):

$$\text{chl-}a = 10^{a+bR}, \quad (7)$$

where $a = 0.592$, $b = -3.607$, and the maximum band $R_{rs}(\lambda)$ ratio $R = \log(R_{rs}[443] > R_{rs}[488]/R_{rs}[555])$.

## 3 Results and discussion

### 3.1 Empirical relationships between $F_L$ and IOPs

$F_L$ was quantified empirically by analyzing the correlation using the $a_{ph}(\lambda)$ ratios $a_{ph}(443)/a_{ph}(667)$ and $a_{ph}(488)/a_{ph}(555)$, and $\gamma$ (Fig. 2a–c). The $a_{ph}(443)/a_{ph}(667)$ value was identified as the $a_{ph}(\lambda)$ ratio because it can roughly express the ratio of total algal pigments to total chl-*a*: light at 443 nm is absorbed by most phytoplankton pigments (chlorophylls, photosynthetic and non-photosynthetic carotenoids), but light at 667 nm is mainly absorbed only by chl-*a* (Bidigare et al., 1990). In addition, 488 nm is an absorption band for various carotenoids, and 555 nm is the smallest absorption band for algal pigments (Bidigare et al., 1990). Thus, $a_{ph}(488)/a_{ph}(555)$ can be used





BGD
8, 4985–5017, 2011



as an indicator to assess the abundance of carotenoids (the sum of the diagnostic pigments). The statistical relationships between $F_L$ and the IOPs are shown in Table 3. The relationship between $F_L$ and $a_{ph}(443)/a_{ph}(667)$ is similar to that reported by Fishwick et al. (2006) for the Benguella upwelling region. Fishwick et al. (2006) showed that the chl-*a*-to-total-pigment ratio (chl-*a*/TP) is significantly and positively correlated with $a_{ph}(676)/a_{ph}(440)$ (note that this is the inverse of the ratio used in this study). Diatoms and dinoflagellates, which are generally classified as microphytoplankton (Vidussi et al., 2001), exhibited higher values of chl-*a*/TP and $a_{ph}(676)/a_{ph}(440)$ than smaller phytoplankton groups, that is, flagellates. The total-pigment-to-chl-*a* ratio roughly indicated by $a_{ph}(443)/a_{ph}(667)$ in this study was significantly correlated with dominant cell size in the study area (Fig. 2a). Since a similar relationship with $F_L$ was also found for $a_{ph}(488)/a_{ph}(555)$, it can be said that detection of the abundance of accessory pigments is important for optically assessing the cell size structure of the phytoplankton community. The effect of pigmentation is an important factor that reflects the cell size structure of a phytoplankton community (Ciotti et al., 2002). However, it does not represent the true cell size compositions because the $a_{ph}(\lambda)$ ratios actually reflect the algal pigment composition, which tends to vary with their cell size. Therefore, the use of the $a_{ph}(\lambda)$ ratio as an independent variable in the SDM leads to overestimation of $F_L$ when groups of small phytoplankton, such as small-sized diatoms, which do not contain many carotenoids compared to autotrophic flagellates (Wright and Jeffrey, 2006), are dominant in the water. Although high $F_L$ with a low $a_{ph}(\lambda)$ ratios co-occurs with high fucoxanthin (Fuco/TAP), communities of small phytoplankton containing relatively high Fuco/TAP ratios (which are expected to be small diatoms) are also found at low $F_L$ with a low $a_{ph}(\lambda)$ ratio (dotted circle in Fig. 2a,b). Thus, to derive $F_L$ more accurately using a model, the optical properties of small-sized diatoms must be considered. One way to distinguish such small-sized diatoms is to use $\gamma$.

Figure 2c shows the relationship between $F_L$ and $\gamma$. We obtained a higher correlation between them than between $F_L$ and the $a_{ph}(\lambda)$ ratios (Table 3). Note that high Fuco/TAP groups do not tend to gather as seen in Fig. 2a,b: instead, they are evenly distributed





BGD
8, 4985–5017, 2011



in Fig. 2c except in the high $F_L$ domain. Montes-Hugo et al. (2008) showed a similar relationship between dominant phytoplankton size and $\gamma$ for the Western Antarctic Peninsula region. They demonstrated that $\gamma$ can be a good indicator for determining the dominance of microphytoplankton, although they defined the cell size as larger than 20 µm. Our results suggest that micro- and nanophytoplankton in the present study (defined as larger than 5 µm) can also be approximately estimated by $\gamma$ in this region (Fig. 2c). The problem with using $\gamma$ as a variable to derive $F_L$ is that the presence of NAPs might cause errors. In that case, extraction of the backscattering coefficient of phytoplankton cells is required for accurate estimation of $F_L$, though that would be difficult at present.

The $a_{ph}(\lambda)$ ratio determined by pigment composition indicates the physiological properties, which tend to vary with phytoplankton cell size (Ciotti et al., 2002). On the other hand, $\gamma$ is determined by the average diameter of suspended particles including NAPs and is influenced by the geometry of the phytoplankton cells rather than their pigment composition. Hence, although the $a_{ph}(\lambda)$ ratio and $\gamma$ are not completely independent, their variations with $F_L$ can be different.

Despite the problems with deriving $F_L$ using the IOPs mentioned above, a multiple regression model using both the $a_{ph}(\lambda)$ ratio and $\gamma$ as independent variables is an effective method for deriving the true algal size. To improve the SDM's accuracy, we selected the multiple logistic regression model and fitted to the in situ $F_L$, $a_{ph}(\lambda)$ ratio, and $\gamma$ data,

$$F_L = \frac{1}{1+\exp\left[-\left(a\frac{a_{ph}(\lambda_1)}{a_{ph}(\lambda_2)}+b\gamma+c\right)\right]} \times 100\,[\%], \quad (8)$$

where $a$, $b$ and $c$ represent the regression coefficients of the model, as listed in Table 4, and $\lambda_1$ and $\lambda_2$ represent the wavelengths of the $a_{ph}(\lambda)$ ratio, which can indicate algal pigmentation. Note that a logistic regression model is suitable for representing the variation in $F_L$ because it has an upper limit of 100 % and a lower limit of 0 %. Using the model, we successfully avoided unrealistic values of $F_L$ (such as negative values





BGD
8, 4985–5017, 2011



and those higher than 100 %) when we applied it to unknown remotely sensed ocean color data. Thus, we proposed application of Eq. (8) as the SDM to satellite remote sensing data for deriving $F_L$.

### 3.2 SDM validation

The accuracy of the SDM was validated using in situ $R_{rs}(\lambda)$ data to avoid the effect of atmospheric correction errors or surface effects such as whitecaps and sun glint. In this study, $a_{ph}(488)/a_{ph}(555)$ was used as the SDM input (Eq. 8) because the estimation accuracy of $a_{ph}(667)$ could be worse compared with that at shorter wavelengths ($< 555$ nm) because $a_t(\lambda)$ is dominated by $a_w(\lambda)$. Figure 3 compares the retrieved $F_L$ and $F_L$ sampled in situ at the sea surface. Fifty-five data points were used for this examination (distinct from the data used for SDM development). The SDM successfully derived an $F_L$ value of 69 % for all data within an error range of ±20 %. A comparison of the SDM's accuracy with that of other phytoplankton size-retrieving models using the root mean square error (RMSE) (Ciotti and Bricaud, 2006; Mouw and Yoder, 2010) revealed that the SDM exhibited a slightly worse RMSE of 22.7 % than that found by Ciotti and Bricaud (2006) (RMSE 17.2 %) and Mouw and Yoder (2010) (RMSE 12.6 %). However, the SDM successfully derived $F_L$ with sufficient accuracy even in the Chukchi Sea, which is known as optically complex water owing to the high proportion of $a_{CDOM}(\lambda)$ to $a_t(\lambda)$ (Pegau, 2002; Wang et al., 2005). Although the SDM's estimation accuracy for $F_L$ can be improved, the SDM has the advantage of deriving phytoplankton size structures by a ratio expressing the existence of nano- and microphytoplankton using a simple equation (Eq. 8). Since the SDM was developed empirically using in situ IOPs, the $a_{ph}(\lambda)$ ratio and $\gamma$, which co-vary with the phytoplankton size, accurate estimation of the IOPs results in successful $F_L$ derivation. In addition, our result shows that $a_{ph}(443)/a_{ph}(667)$, which reflects the ratio of the total pigment concentration (sum of AP and chl-*a*) to the chl-*a* concentration, showed a higher correlation with $F_L$ than $a_{ph}(488)/a_{ph}(555)$. Thus, we believe that if accurate remote sensing of $a_{ph}(\lambda)$ in red light, such as $a_{ph}(667)$, could be achieved with sufficient confidence, the accuracy of





BGD
8, 4985–5017, 2011



$F_L$ estimation will improve. Although several studies have tried to derive $a_{ph}(\lambda)$ for red light (e.g., Simis et al., 2005; Zhang et al., 2010), their success can be limited to cases of high $a_{ph}(\lambda)$ in land water. Therefore, $a_{ph}(488)/a_{ph}(555)$ was used as an independent variable of the SDM in this study.

### 3.3 Application of SDM to satellite remote sensing

Figure 4a,b shows the spatial distribution of $F_L$ in the Western Arctic during August 2006 and August 2007. August is the most stratified season in the Western Arctic. A high proportion of larger phytoplankton assemblages were observed in the continental shelf region around the Bering Strait. In contrast, low $F_L$ was observed in the outer shelf and the Bering Basin, which are believed to be nutrient-depleted or iron-limited regions (Aguilarislas et al., 2007). Hill et al. (2005) also reported that similar distribution patterns of size-fractionated chl-*a* (> 5µm) in the Chukchi and Eastern Beaufort Sea in summer 2002. In this study, we found different $F_L$ distributions in 2006 and 2007. The distribution of extremely high $F_L$ (~ 90 %) had a greater extent in 2007 than in 2006 around the Bering Strait; in contrast, lower $F_L$ values (~ 40 %) were distributed more broadly in the Northern Chukchi Sea shelf (~ 67° N) (Fig. 4a,b). There should be some environmental reasons for the subsequent changes in the distribution of $F_L$ through the time series. Satellite estimation of $F_L$ can be used for examining how the dominant size of phytoplankton communities in the Western Arctic has responded spatiotemporally to climate change such as the reduction in sea ice. As a preliminary application of the SDM analysis, Fig. 5a–c shows frequency histograms of $F_L$, log-transformed chl-*a*, and SST in the box defined in Fig. 4a,b (60–72° N, 166–172° W) for August 2006 and August 2007. A *t*-test was used to examine the difference in the mean values for 2006 and 2007 (Table 5). Although there was no significant difference in chl-*a* between 2006 and 2007 ($p > 0.25$) (Fig. 5b), $F_L$ in 2007 was significantly lower than in 2006 ($p < 0.025$) (Table 5, Fig. 5a). On the other hand, the SST in 2007 was significantly higher than that in 2006 ($p < 0.005$) (Fig. 5c). Sea ice was distributed in the Northern Chukchi Sea around 72° N in 2006, but no sea ice cover was found in





BGD
8, 4985–5017, 2011



2007 (Fig. 4a,b). The Arctic sea ice cover in summer 2007 was the lowest ever observed (http://www.eorc.jaxa.jp/en/imgdata/topics/2007/tp071024.html). Furthermore, Woodgate et al. (2010) noted that the heat flux into the Arctic Ocean through the Bering Strait in 2007 was greatest during the observation period (1991–2007) and consequently caused the SST increase in 2007. The preliminary result of this study indicates that phytoplankton cell size rather than chl-*a* can be responsive to ocean warming from 2006 to 2007 in the study region (Fig. 5). However, it is not clear whether the shift in the cell size of the algal community observed by the satellite remote sensing is due to the advection of smaller phytoplankton communities from the southern part of the region or to the fact that groups of smaller phytoplankton could be better adapted than groups of larger ones to sudden ocean warming which was showed in incubation experiments (e.g., Noiri et al., 2005; Hare et al., 2008). Further analysis is required to assess the effect of changes in the ocean environment on the structure of phytoplankton assemblages over a longer time period. However, the SDM established its suitability for monitoring the spatiotemporal distribution of algal size structures by retrieving $F_L$ independent of chl-*a* (Table 5, Fig. 5a,b). This result demonstrates an advantage of the SDM compared with the chl-*a*-based PFT algorithms proposed in several studies (e.g., Uitz et al., 2006; Brewin et al., 2010).

## 4 Conclusions

This study proposes an SDM for deriving phytoplankton cell size structures from space and describes the first experiment that uses multiple optical property inputs; the $a_{ph}(\lambda)$ ratio indicates the tendency of $F_L$ variation based on physiological optical theory and that of $\gamma$ based on geometrical optical theory. Empirical approaches using either the $a_{ph}(\lambda)$ ratio or $\gamma$ encounter problems with the estimation of $F_L$; the use of the $a_{ph}(\lambda)$ ratio causes overestimation when small diatoms ($< 5\,\mu m$) dominate and $\gamma$ might be optically influenced by NAPs. To overcome these problems, a multiple logistic regression model that regards the $a_{ph}(\lambda)$ ratio and $\gamma$ as the independent variables was adopted as the SDM. The advantage of this SDM is that it can retrieve the proportion of $> 5\,\mu m$





BGD
8, 4985–5017, 2011



phytoplankton cells existing in the water, independent of the dominant phytoplankton groups. However, the SDM was developed using only data obtained on a summer cruise of the Oshoro-maru 2007 (OS180). The SDM still needs improvements, such as considerations of seasonal variability of the IOPs and also improved IOP estimation accuracy. However, it performed with sufficient accuracy when applied to unknown data even in high-$a_{CDOM}(\lambda)$ optically complex water in which the ecosystem's structure has been changing with ocean warming (Grebmeier et al., 2006b). We conclude that application of the SDM to satellite remote sensing has the potential to advance knowledge of the response of phytoplankton to recent climate change and their contribution to the food web in the shelf region in the Chukchi and the Bering Seas.

*Acknowledgement.* We sincerely acknowledge the captains and crews of the T/S *Oshoro-maru*, R/V *Mirai*, and R/V *Hakuho-maru* for their cooperation during the cruises. We thank the staffs of JAMSTEC and Marine Work Japan, Ltd., for obtaining and analyzing the data. We express our appreciation the Distributed Active Archive Center (DAAC) at the Goddard Space Flight Center (GSFC) for the production and distribution of satellite data. This study was supported in part by the Japan Society for the Promotion of Science (JSPS) and the IARC/JAXA Information System (IJIS).

## References

Aguilar-Islas, A., Hurst, M., Buck, K., Sohst, B., Smith, G., Lohan, M., and Bruland, K.: Micro- and macronutrients in the Southeastern Bering Sea: insight into iron-replete and iron-depleted regimes, Prog. Oceanogr., 73(2), 99–126, doi:10.1016/j.pocean.2006.12.002, 2007.

Aiken, J., Fishwick, J. R., Lavender, S., Barlow, R., Moore, G. F., Sessions, H., Bernard, S., Ras, J., and Hardman-Mountford, N.: Validation of MERIS reflectance and chlorophyll during the BENCAL cruise October 2002: preliminary validation of new demonstration products for phytoplankton functional types and photosynthetic parameters, Int. J. Remote Sens., 28(3–4), 497–516, doi:10.1080/01431160600821036, 2007.

Alvain, S., Moulin, C., Dandonneau, Y., and Bréon, F.: Remote sensing of phytoplankton groups





BGD
8, 4985–5017, 2011



in case 1 waters from global SeaWiFS imagery, Deep-Sea Res. Pt. I, 52(11), 1989–2004, 2005.
Arrigo, K., van Dijken, G., and Pabi, S.: Impact of a shrinking Arctic ice cover on marine primary production, Geophys. Res. Lett., 35(19), L19603, 2008.
Bidigare, R. R., Ondrusek, M. E., Morrow, J. H., and Kiefer, D. A.: In-vivo absorption properties of algal pigments, Proc. SPIE, 1302, 290–302, 1990.
Brewin, R. J. W., Sathyendranath, S., Hirata, T., Lavender, S. J., Barciela, R. M., and Hardman-Mountford, N. J.: A three-component model of phytoplankton size class for the Atlantic Ocean, Ecol. Model., 221(11), 1472–1483, doi:10.1016/j.ecolmodel.2010.02.014, 2010.
Bricaud, A. and Morel, A.: Light attenuation and scattering by phytoplanktonic cells: a theoretical modeling, Appl. Opt., 25(4), 571–580, doi:10.1364/AO.25.000571, 1986.
Carder, K., Chen, F., Lee, Z., Hawes, S., and Kamykowski, D.: Semianalytic moderate-resolution imaging spectrometer algorithms for chlorophyll-*a* and absorption with bio-optical domains based on nitrate-depletion temperatures, J. Geophys. Res., 104(C3), 5403–5421, 1999.
Chisholm, S. W.: Phytoplankton size, in: Primary Productivity and Biogeochemical Cycles in the Sea, edited by: Falkowski, P. G. and Woodhead, A. D., Plenum Press, New York, 213–238, 1992.
Ciotti, A. and Bricaud, A.: Retrievals of a size parameter for phytoplankton and spectral light absorption by colored detrital matter from water-leaving radiances at SeaWiFS channels in a continental shelf region off Brazil, Limnol. Oceanogr.-Meth., 4, 237–253, 2006.
Ciotti, A., Lewis, M., and Cullen, J.: Assessment of the relationships between dominant cell size in natural phytoplankton communities and the spectral shape of the absorption coefficient, Limnol. Oceanogr., 47(2), 404–417, 2002.
Cleveland, J. and Weidemann, A.: Quantifying absorption by aquatic particles: a multiple scattering correction for glass-fiber filters, Limnol. Oceanogr., 38(5), 1321–1327, 1993.
Coachman, L. K., Aagaard, K., and Tripp, R. B.: Bering Strait: The Regional Physical Oceanography, Univ. of Washington Press, Seattle, 172 pp., 1975.
Comiso, J.: A rapidly declining perennial sea ice cover in the Arctic, Geophys. Res. Lett., 29(20), 17–11, 2002.
Comiso, J. C., Parkinson, C. L., Gersten, R., and Stock, L.: Accelerated decline in the Arctic sea ice cover, Geophys. Res. Lett., 35(1), L01703, doi:10.1029/2007GL031972, 2008.
Cota, G., Harrison, W., Platt, T., Sathyendranath, S., and Stuart, V.: Bio-optical properties of





BGD
8, 4985–5017, 2011



the Labrador Sea, J. Geophys. Res., 108(C7), 3228, 2003.
Cota, G., Wang, J., and Comiso, J.: Transformation of global satellite chlorophyll retrievals with a regionally tuned algorithm, Remote Sens. Environ., 90(3), 373–377, 2004.
Darecki, M. and Stramski, D.: An evaluation of MODIS and SeaWiFS bio-optical algorithms in the Baltic Sea, Remote Sens. Environ., 89(3), 326–350, 2004.
Feder, H., Jewett, S., and Blanchard, A.: Southeastern Chukchi Sea (Alaska) epibenthos, Polar Biol., 28(4), 402–421, 2005.
Fishwick, J., Aiken, J., Barlow, R., Sessions, H., Bernard, S., and Ras, J.: Functional relationships and bio-optical properties derived from phytoplankton pigments, optical and photosynthetic parameters; a case study of the Benguela ecosystem, J. Mar. Biol. Assoc. UK, 86(06), 1267–1280, 2006.
Grebmeier, J., McRoy, C., and Feder, H.: Pelagic-benthic coupling on the shelf of the Northern Bering and Chukchi seas. 1. Food supply source and benthic biomass Mar. Ecol.-Prog. Ser., 48(1), 57–67, 1988.
Grebmeier, J., Cooper, L., Feder, H., and Sirenko, B.: Ecosystem dynamics of the Pacific-influenced Northern Bering and Chukchi Seas in the Amerasian Arctic, Prog. Oceanogr., 71(2–4), 331–361, 2006a.
Grebmeier, J., Overland, J., Moore, S., Farley, E., Carmack, E., Cooper, L., Frey, K., Helle, J., McLaughlin, F.: A major ecosystem shift in the Northern Bering Sea, Science, 311(5766), 1461, 2006b.
Hare, C. E., Leblanc, K., DiTullio, G. R., Kudela, R. M., Zhang, Y., Lee, P. A., Riseman, S., and Hutchins, D. A.: Consequences of increased temperature and $CO_2$ for phytoplankton community structure in the Bering Sea, Mar. Ecol.-Prog. Ser., 352, 9–16, doi:10.3354/meps07182, 2007.
Hill, V., Cota, G., and Stockwell, D.: Spring and summer phytoplankton communities in the Chukchi and Eastern Beaufort Seas, Deep-Sea Res. Pt. II, 52(24–26), 3369–3385, 2005.
Jeffrey, S. W. and Vesk, M.: Introduction to marine phytoplankton and their pigment signatures, in: Phytoplankton Pigments in Oceanography: Guidelines to Modern Methods, edited by: Jeffrey, S. W., Mantoura, R. F. C., and Wright, S. W., UNESCO Publishing, Paris, 37–84, 1997.
Kishino, M., Takahashi, M., Okami, N., and Ichimura, S.: Estimation of the spectral absorption coefficients of phytoplankton in the sea, B. Mar. Sci., 37(2), 634–642, 1985.
Lalli, C. M., and Parsons, T. R.: Biological Oceanography: an Introduction, Elsevier, New York,





BGD
8, 4985–5017, 2011



314 pp., 1995.
Lee, Z., Carder, K., and Arnone, R.: Deriving inherent optical properties from water color: a multiband quasi-analytical algorithm for optically deep waters, Appl. Opt., 41(27), 5755–5772, 2002.
Lee, Z., Lubac, B., Werdell, J., and Arnone, R.: An Update of the Quasi-Analytical Algorithm (QAA_v5), available at: http://www.ioccg.org/groups/Software_OCA/QAA_v5.pdf. Retrieved from http://www.ioccg.org/groups/software.html, last access: 14 May 2011, 2009.
Lochte, K., Ducklow, H. W., Fasham, M. J. R., and Stienens, C.: Plankton succession and carbon cycling at 47° N 20° W during the JGOFS North Atlantic Bloom Experiment, Deep-Sea Res. Pt. II, 40(1–2), 91–114, 1993.
Lyon, P. and Hoge, F.: The linear matrix inversion algorithm, in: Remote Sensing of Inherent Optical Properties: Fundamentals, Tests of Algorithms, and Applications, edited by: Lee, Z., IOCCG, Dartmouth, 49–56, 2006.
Maffione, R. and Dana, D.: Instruments and methods for measuring the backward-scattering coefficient of ocean waters, Appl. Opt., 36(24), 6057–6067, 1997.
Montes-Hugo, M. A., Vernet, M., Smith, R., and Carder, K.: Phytoplankton size-structure on the western shelf of the Antarctic Peninsula: a remote-sensing approach, Int. J. Remote Sens., 29(3), 801–829, doi:10.1080/01431160701297615, 2008.
Morel, A. and Prieur, L.: Analysis of variations in ocean color, Limnol. Oceanogr., 22(4), 709–722, 1977.
Mouw, C. B. and Yoder, J. A.: Optical determination of phytoplankton size composition from global SeaWiFS imagery, J. Geophys. Res., 115, C12018, 2010.
Noiri, Y., Kudo, I., Kiyosawa, H., Nishioka, J., and Tsuda, A.: Influence of iron and temperature on growth, nutrient utilization ratios and phytoplankton species composition in the Western Subarctic Pacific Ocean during the SEEDS experiment, Prog. Oceanogr., 64, 149–166, doi:10.1016/j.pocean.2005.02.006, 2005.
Pabi, S., van Dijken, G., and Arrigo, K.: Primary production in the Arctic Ocean, 1998–2006, J. Geophys. Res., 113(C8), C08005, 2008.
Parkinson, C. and Cavalieri, D.: Arctic sea ice variability and trends, 1979–2006, J. Geophys. Res., 113(C7), C07003, 2008.
Pegau, W. S.: Inherent optical properties of the central Arctic surface waters, J. Geophys. Res., 107(C), 8035, doi:10.1029/2000JC000382, 2002.
Pegau, S., Ronald, J., Zaneveld, V., Mitchell, B. G., Mueller, J. L., Kahru, M., and Wieland, J.:





BGD
8, 4985–5017, 2011



Ocean optics protocols for satellite ocean color sensor validation, revision 4, in: Inherent Optical Properties: Instruments, Characterizations, Field Measurements and Data Analysis Protocols (Vol. IV), edited by: Mueller, J. L., Fargion, G. S., and McClain, C. R., Goddard Space Flight Cent., Greenbelt, 1–83, 2003.

Sathyendranath, S., Cota, G., Stuart, V., Maass, H., and Platt, T.: Remote sensing of phytoplankton pigments: a comparison of empirical and theoretical approaches, Int. J. Remote Sens., 22(2–3), 249–273, 2001.

Sathyendranath, S., Watts, L., Devred, E., Platt, T., Caverhill, C., and Maass, H.: Discrimination of diatoms from other phytoplankton using ocean-colour data, Mar. Ecol.-Prog. Ser., 272, 59–68, 2004.

Shimada, K., Kamoshida, T., Itoh, M., Nishino, S., Carmack, E., McLaughlin, F., Zimmermann, S., and Proshutinsky, A.: Pacific Ocean inflow: influence on catastrophic reduction of sea ice cover in the Arctic Ocean, Geophys. Res. Lett., 33(7), L08605, 2006.

Simis, S., Peters, S., and Gons, H.: Remote sensing of the cyanobacterial pigment phycocyanin in turbid inland water, Limnol. Oceanogr., 50(1), 217–245, 2005.

Smith, R. and Baker, K.: Optical properties of the clearest natural waters (200–800 nm), Appl. Opt., 20(2), 177–184, 1981.

Smyth, T., Moore, G., Hirata, T., and Aiken, J.: Semianalytical model for the derivation of ocean color inherent optical properties: description, implementation, and performance assessment, Appl. Opt., 45(31), 8116–8131, 2006.

Springer, A. M. and McRoy, C. P.: The paradox of pelagic food webs in the Northern Bering Sea – III. Patterns of primary productivity, Cont. Shelf Res., 13, 575–599, 1993.

Stramski, D., Bricaud, A., and Morel, A.: Modeling the inherent optical properties of the ocean based on the detailed composition of the planktonic community, Appl. Opt., 40, 2929–2945, 2001.

Sullivan, J. M. and Twardowski, M. S.: Angular shape of the oceanic particulate volume scattering function in the backward direction, Appl. Opt., 48(35), 6811–6819, 2009.

Suzuki, K., Hinuma, A., Saito, H., Kiyosawa, H., Liu, H., Saino, T., and Tsuda, A.: Responses of phytoplankton and heterotrophic bacteria in the northwest subarctic Pacific to in situ iron fertilization as estimated by HPLC pigment analysis and flow cytometry, Prog. Oceanogr., 64(2–4), 167–187, 2005.

Turner, S. M., Malin, G., Liss, P. S., Harbour, D. S., and Holligan, P. M.: The seasonal variation of dimethyl sulfide and dimethylsulfoniopropionate concentrations in nearshore waters, Limnol.





BGD
8, 4985–5017, 2011



Oceanogr., 33, 364–375, 1988.
Uitz, J., Claustre, H., Morel, A., and Hooker, S.: Vertical distribution of phytoplankton communities in open ocean: an assessment based on surface chlorophyll, J. Geophys. Res., 111(C8), C08005, 2006.
Vaillancourt, R. D., Brown, C. W., Guillard, R. R. L., and Balch, W. M.: Light backscattering properties of marine phytoplankton: relationships to cell size, chemical composition and taxonomy, J. Plankton Res., 26(2), 191–212, doi:10.1093/plankt/fbh012, 2004.
Vidussi, F., Claustre, H., Manca, B., Luchetta, A., and Marty, J.: Phytoplankton pigment distribution in relation to upper thermocline circulation in the eastern Mediterranean Sea during winter, J. Geophys. Res., 106(C9), 19939, 2001.
Wang, J. and Cota, G.: Remote-sensing reflectance in the Beaufort and Chukchi Seas: observations and models, Appl. Opt., 42(15), 2754–2765, 2003.
Wang, J., Cota, G., and Ruble, D.: Absorption and backscattering in the Beaufort and Chukchi Seas, J. Geophys. Res., 110(C4), C04014, 2005.
Welschmeyer, N.: Fluorometric analysis of chlorophyll a in the presence of chlorophyll-*b* and pheopigments, Limnol. Oceanogr., 39(7), 1985–1992, 1994.
Woodgate, R. A., Aagaard, K., and Weingartner, T. J.: Interannual changes in the Bering Strait fluxes of volume, heat and freshwater between 1991 and 2004, Geophys. Res. Lett., 33, 15609, doi:10.1029/2006GL026931, 2006.
Woodgate, R. A., Weingartner, T., and Lindsay, R.: The 2007 Bering Strait oceanic heat flux and anomalous Arctic sea-ice retreat, Geophys. Res. Lett., 37, 01602, doi:10.1029/2009GL041621, 2010.
Wright, S. W. and Jeffrey, S. W.: Pigment markers for phytoplankton production, in: Marine Organic Matter: Biomarkers, Isotopes and DNA, edited by: Volkmann, J. K., Springer-Verlag, Berlin, 71–104, 2006.
Yoder, J. A. and Kennelly, M. A.: What have we learned about ocean variability from satellite ocean color images?, Oceanography, 19(1), 152, 2006.
Zehr, J. and Carpenter, E.: New perspectives on nitrogen-fixing microorganisms in tropical and subtropical oceans, Trends Microbiol., 8, 68–73, 2000.
Zhang, Y., Feng, L., Li, J., Luo, L., Yin, Y., Liu, M., and Li, Y.: Seasonal-spatial variation and remote sensing of phytoplankton absorption in Lake Taihu, a large eutrophic and shallow lake in China, J. Plankton Res., 32(6), 1023–1037, doi:10.1093/plankt/fbq039, 2010.





BGD
8, 4985–5017, 2011



**Table 1.** List of symbols and units.

| Abbreviation | Definition | Unit |
|---|---|---|
| $a_t$ | Total absorption coefficient | $m^{-1}$ |
| $a_w$ | Water absorption coefficient | $m^{-1}$ |
| $a_p$ | Particle absorption coefficient | $m^{-1}$ |
| $a_{NAP}$ | Non-algal particle absorption coefficient | $m^{-1}$ |
| $a_{CDOM}$ | CDOM absorption coefficient | $m^{-1}$ |
| $a_{dg}$ | The sum of $a_{NAP}$ and $a_{CDOM}$ | $m^{-1}$ |
| $a_{ph}$ | Phytoplankton absorption coefficient | $m^{-1}$ |
| $b_b$ | Backscattering coefficient | $m^{-1}$ |
| $b_{bp}$ | Particle backscattering coefficient | $m^{-1}$ |
| $b_{bw}$ | Water backscattering coefficient | $m^{-1}$ |
| $\beta$ | Volume scattering function | $sr^{-1}\,m^{-1}$ |
| $E_d$ | Downwelling irradiance | $W\,m^{-2}\,nm^{-1}$ |
| $\gamma$ | Spectral slope of $b_{bp}$ | $nm^{-1}$ |
| $L_u$ | Upwelling radiance | $W\,m^{-2}\,sr^{-1}\,\mu m^{-1}$ |
| $L_w$ | Water-leaving radiance | $W\,m^{-2}\,sr^{-1}\,\mu m^{-1}$ |
| $\lambda$ | Wavelength | nm |
| $R_{rs}$ | Surface remote sensing reflectance | $sr^{-1}$ |
| OD | Optical density | |
| $S$ | Spectral slope of $a_{dg}$ | $nm^{-1}$ |
| $F_L$ | Phytoplankton size index | % |
| AP | Accessory pigment | |
| DP | Diagnostic pigment | |
| TAP | Total accessory pigment concentration | $mg\,m^{-3}$ |
| TP | Total pigment concentration | $mg\,m^{-3}$ |





BGD
8, 4985–5017, 2011



**Table 2.** Major taxonomically significant pigments in phytoplankton groups and their abbreviations (Jeffrey and Vesk, 1997) and definitions of four major algal assemblages determined by pigment composition (Aiken et al., 2007).

| Pigment | Specificity |
|---|---|
| Peridinin (Peri) | Dinoflagellates |
| 19′-butanoyloxyfucoxanthin (19′-BF) | Haptophytes 3 and 4, chrysophytes |
| Fucoxanthin (Fuco) | Diatoms, haptophytes1, 2, 3 and 4, chrysophytes |
| 19′-hexanoyloxyfucoxanthin (19′-HF) | Haptophytes3 and 4 |
| Alloxanthin (Allo) | Chrysophytes |
| Zeaxanthin (Zea) | Chlorophytes |
| Chlorophyll *b* (chl-*b*) | Chlorophytes |
| Chlorophyll *a* (chl-*a*) | All groups |
| Fuco/TAP | Diatoms |
| Peri/TAP | Dinoflagellates |
| (19′-BF+19′-HF+Allo+chl-*b*)/TAP | Flagellates |
| Zea/TAP | Procaryotes |





BGD
8, 4985–5017, 2011



**Table 3.** Determination coefficients ($r^2$) between $F_L$ and IOPs, $a_{ph}(443)/a_{ph}(667)$, $a_{ph}(488)/a_{ph}(555)$, and $\gamma$. All $p$-values were less than 0.01.

| | $a_{ph}(443)/a_{ph}(667)$ | $a_{ph}(488)/a_{ph}(555)$ | $\gamma$ |
|---|---|---|---|
| Slope | −32.43 | −15.07 | −19.15 |
| Intercept | 119.6 | 89.20 | 98.26 |
| $r^2$ | 0.58 | 0.52 | 0.60 |
| $N$ | 77 | 77 | 77 |





BGD
8, 4985–5017, 2011



**Table 4.** Regression coefficients for SDM (Eq. 8) when $a_{ph}(443)/a_{ph}(667)$ and $\gamma$ were used, and when $a_{ph}(488)/a_{ph}(555)$ and $\gamma$ were used.

| | $a_{ph}(443)/a_{ph}(667)$ and $\gamma$ | $a_{ph}(488)/a_{ph}(555)$ and $\gamma$ |
|---|---|---|
| $a$ | −1.056 | −0.570 |
| $b$ | −0.591 | −0.565 |
| $c$ | 4.001 | 3.175 |





BGD
8, 4985–5017, 2011



**Table 5.** Statistical difference in monthly averaged $F_L$, chl-*a* and SST between August 2006 and August 2007. Values in the box (60–72° N, 166–172° W, Fig. 4) were averaged. Values in parentheses are standard deviation.

| Year | $F_L$ | chl-*a* | SST |
|---|---|---|---|
| 2006 ave. (SD) | 55.17 (15.61) | 1.75 (2.44) | 7.21 (1.96) |
| 2007 ave. (SD) | 52.88 (17.11) | 2.14 (3.10) | 10.01 (1.55) |
| *p*-value | $< 0.025$ | $> 0.1$ | $< 0.0025$ |





BGD
8, 4985–5017, 2011



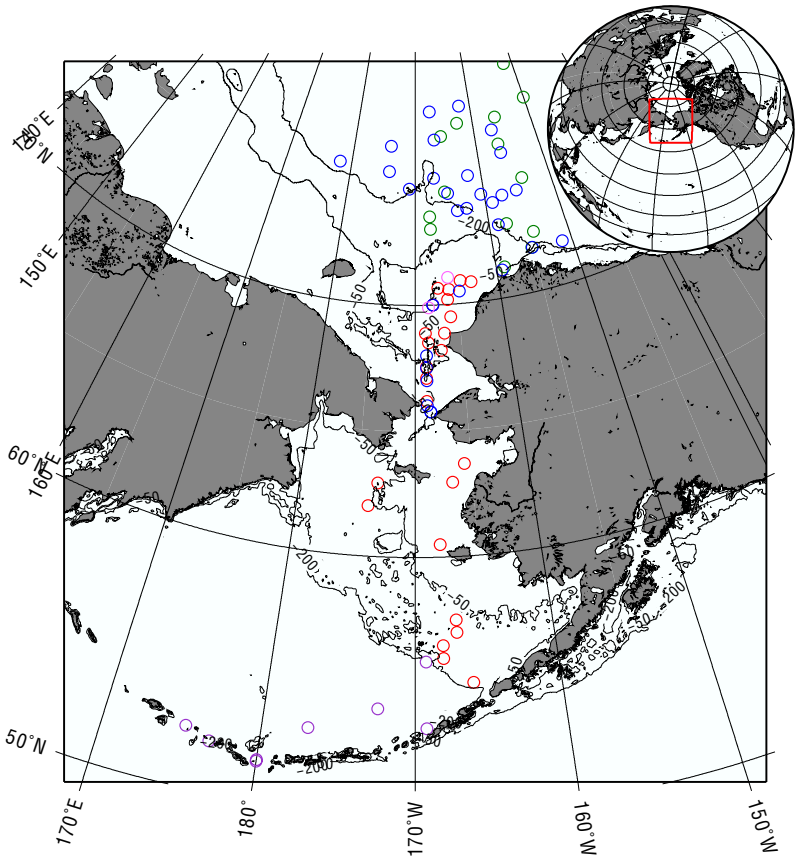


**Fig. 1.** Location of 75 stations that in situ data were obtained for this study. Data for SDM development were sampled during the OS180 (red circles) and those for SDM validation were sampled during the OS190 (pink circles), KH09-4 (purple circles) and MR10-05 (blue circles). Bathymetry contours indicated are 50- and 200-m intervals.





BGD
8, 4985–5017, 2011



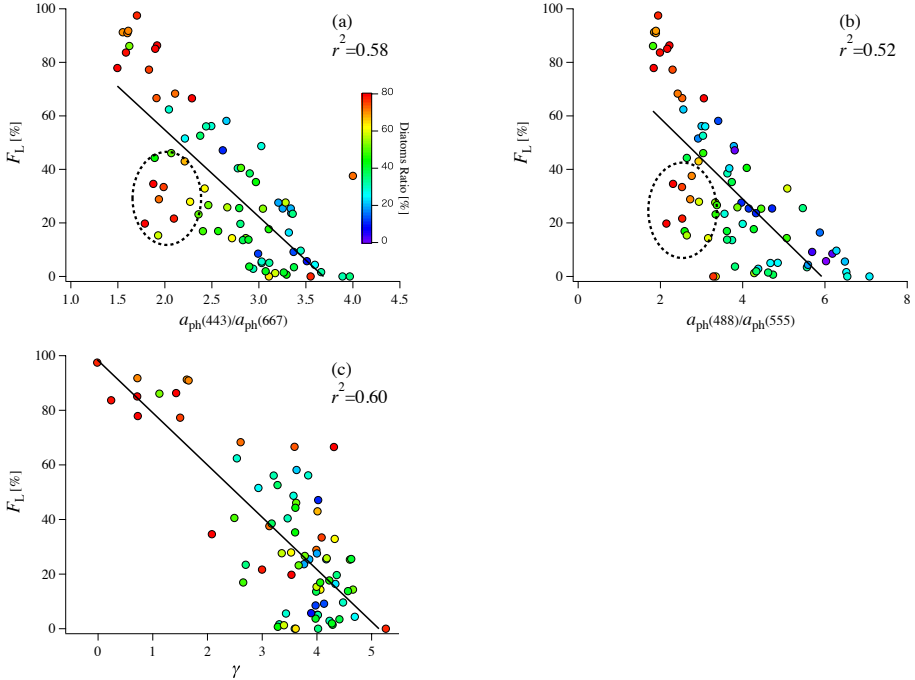


**Fig. 2.** Variation of in situ $F_L$ as a function of **(a)** in situ $a_{ph}(443)/a_{ph}(667)$, **(b)** in situ $a_{ph}(488)/a_{ph}(555)$ and **(c)** in situ $\gamma$. Colors in each plot correspond to diatom fraction calculated by HPLC pigment composition (Aiken et al., 2007).





BGD
8, 4985–5017, 2011



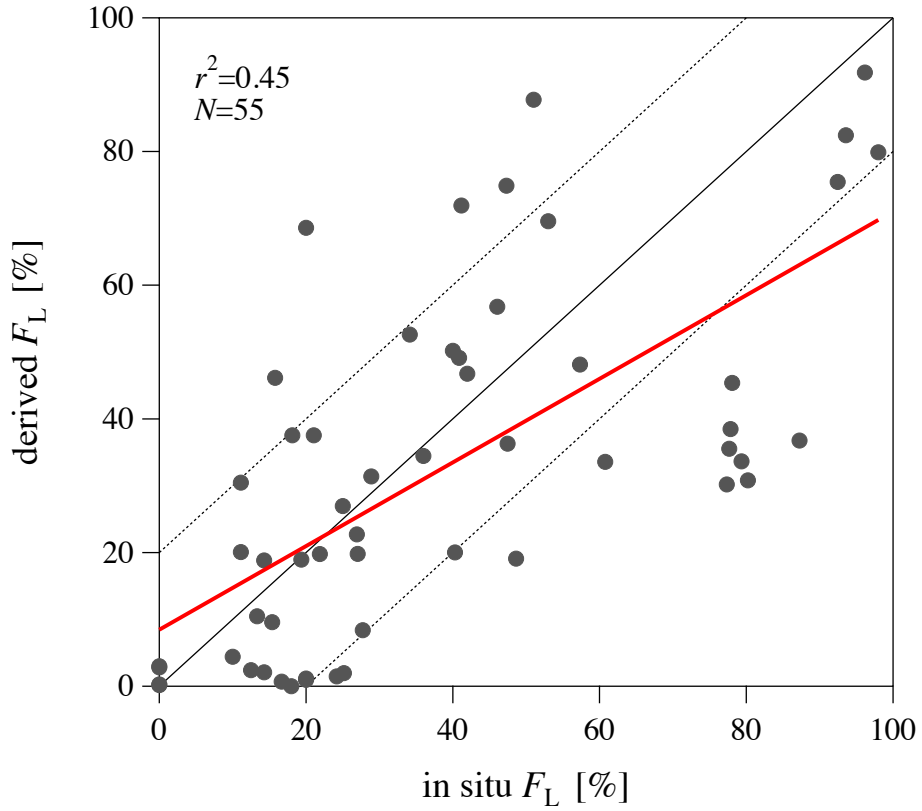


**Fig. 3.** Comparison of SDM-derived $F_L$ and in situ $F_L$ ($r^2 = 0.45$, $p < 0.0001$, $N = 55$). Solid red line represents the regression line, the solid black line indicates the 1 : 1 line, and the dashed lines indicate the ±20 % range with respect to the 1 : 1 line.





BGD
8, 4985–5017, 2011



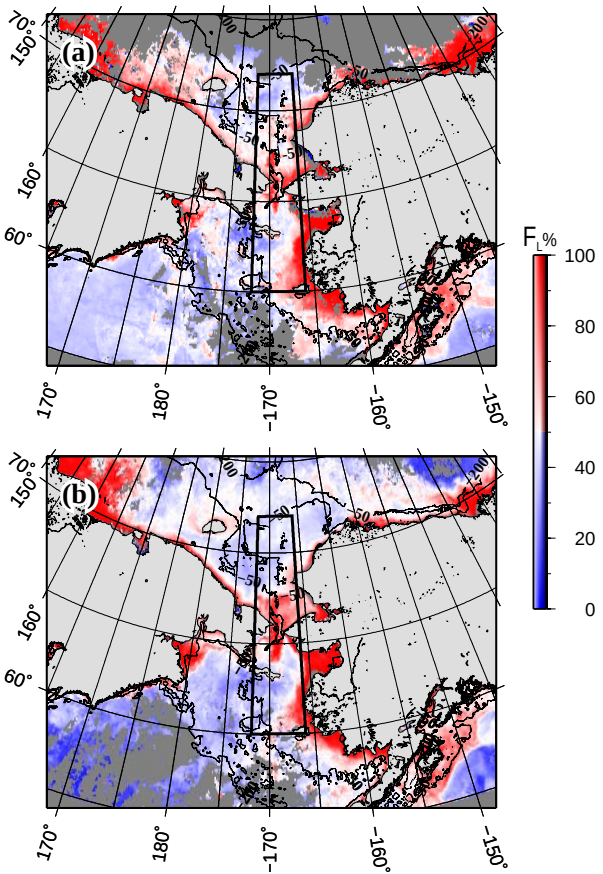


**Fig. 4.** Satellite-retrieved map of $F_L$ in the study region for **(a)** August 2006 and **(b)** August 2007. Gray indicates the presence of clouds or sea ice. Frames located at 60–72° N, 166–172° W indicate the area for which statistical analysis was performed (Table 5, Fig. 5).





BGD
8, 4985–5017, 2011



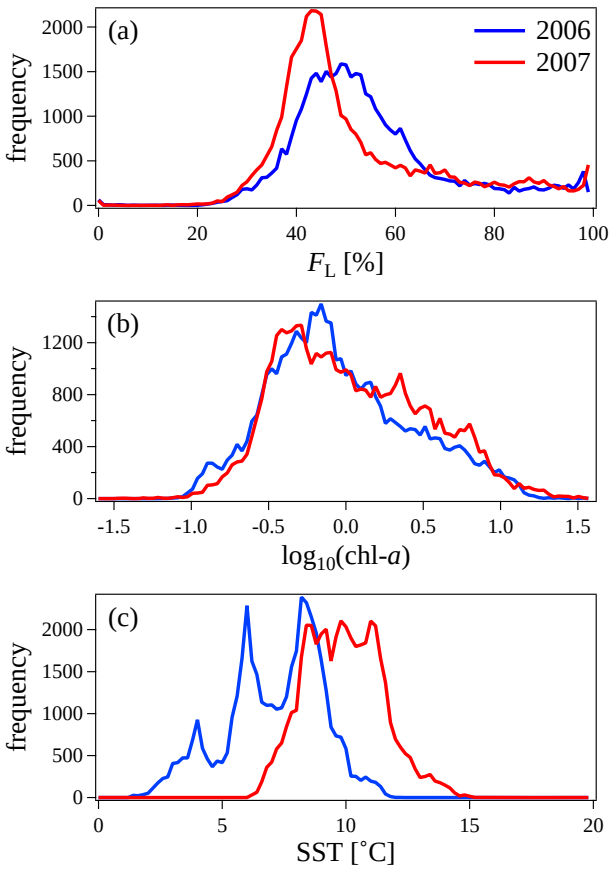


**Fig. 5.** Histograms of **(a)** $F_L$, **(b)** log-transformed chl-*a* and **(c)** SST in the area defined in the shelf region (Fig. 4). Blue and red lines indicate the observations of August 2006 and of August 2007, respectively.





BGD
8, 4985–5017, 2011